

Effects of shallow carbon and deep N++ layer on the radiation hardness of IHEP-IME LGAD sensors

Mengzhao Li*, Yunyun Fan*, Xuwei Jia, Han Cui, Zhijun Liang, Mei Zhao, Tao Yang, Kewei Wu, Shuqi Li, Chengjun Yu, Bo Liu, Wei Wang, Xuan Yang, Yuhang Tan, Xin Shi, J. G. da Costa, Yuekun Heng, *Member, IEEE*, Gaobo Xu, Qionghua Zhai, Gangping Yan, Mingzheng Ding, Jun Luo, Huaxiang Yin, Junfeng Li, Alissa Howard, Gregor Kramberger

Abstract—Low Gain Avalanche Diode (LGAD) is applied for the High-Granularity Timing Detector (HGTD), and it will be used to upgrade the ATLAS experiment. The first batch IHEP-IME LGAD sensors were designed by the Institute of High Energy Physics (IHEP) and fabricated by the Institute of Microelectronics (IME). Three IHEP-IME sensors (W1, W7 and W8) were irradiated by the neutrons up to the fluence of $2.5 \times 10^{15} \text{ n}_{\text{eq}}/\text{cm}^2$ to study the effect of the shallow carbon and deep N++ layer on the irradiation hardness. Taking W7 as a reference, W1 has an extra shallow carbon applied, and W8 has a deeper N++ layer. The leakage current, the collected charge and timing resolution of the three IHEP-IME sensors measured from the Beta telescope test all meet the HGTD requirements ($<125 \mu\text{A}/\text{cm}^2$, $>4 \text{ fC}$ and $<70 \text{ ps}$ after $2.5 \times 10^{15} \text{ n}_{\text{eq}}/\text{cm}^2$ irradiation fluence). The W1 sensor with shallow carbon is the most radiation hardness, while the W8 sensor with the deep N++ layer showed the worst radiation hardness.

Index Terms—LGAD, Carbon implantation, Irradiation, Beta telescope, Timing resolution, HGTD

I. INTRODUCTION

LOW Gain Avalanche Diode (LGAD) is the choice for the High Granularity Timing Detector (HGTD) [1], [2], which is a thin N-on-P silicon sensor with a highly doped P+ layer inserted between N++ and p-type bulk, as shown in Fig. 1. The P+ layer creates a high field and acts as a gain layer. The LGAD sensor has a good timing resolution and moderate position resolution ability. One of the important applications is the upgrade of the ATLAS experiments at the High-Luminosity Large Hadron Collider (HL-LHC) [1]–[3]. The LGAD sensor is required to reach 70 ps timing resolution

This work was supported by the National Natural Science Foundation of China (No.11961141014), the State Key Laboratory of Particle Detection and Electronics (No.SKLPDE-ZZ-202001), the Hundred Talent Program of the Chinese Academy of Sciences (Y6291150K2), the CAS Center for Excellence in Particle Physics (CCEPP), the Scientific Instrument Developing Project of the Chinese Academy of Sciences (No.ZDKYYQ20200007).

Mengzhao Li*, Yunyun Fan*, Xuwei Jia, Han Cui, Zhijun Liang, Mei Zhao, Tao Yang, Kewei Wu, Shuqi Li, Chengjun Yu, Bo Liu, Wei Wang, Xuan Yang, Yuhang Tan, Xin Shi, J. G. da Costa, Yuekun Heng are with the Institute of High Energy Physics, Chinese Academy of Sciences, Beijing 10049, China (e-mail: Zhijun Liang (liangzj@ihep.ac.cn), Mei Zhao (zhaomei@ihep.ac.cn)), and Mengzhao Li, Xuwei Jia, Han Cui, Tao Yang, Kewei Wu, Shuqi Li, Chengjun Yu, Yuhang Tan, Yuekun Heng are also with the School of Physical Sciences, University of Chinese Academy of Sciences, Beijing 100049, China.

Gaobo Xu, Qionghua Zhai, Gangping Yan, Mingzheng Ding, Jun Luo, Huaxiang Yin, Junfeng Li are with the Institute of Microelectronics, Chinese Academy of Sciences, Beijing 100029, China.

Alissa Howard, Gregor Kramberger are with the Jozef Stefan Institute, SI-1000 Ljubljana, Slovenia.

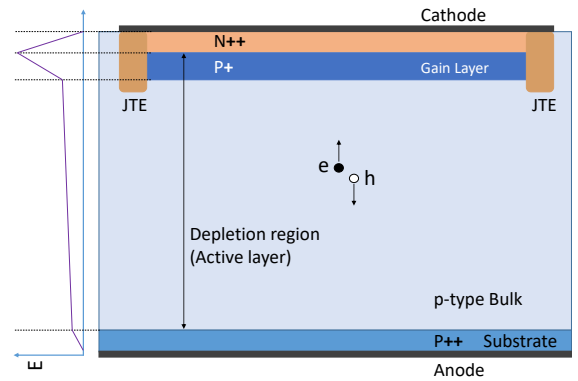


Fig. 1. Schematic for the LGAD sensors.

after irradiation up to $2.5 \times 10^{15} \text{ n}_{\text{eq}}/\text{cm}^2$, and the collected charge is also required to be larger than 4 fC [1].

Ref. [4]–[11] reported the radiation performance of HPK, CNM and IHEP-NDL LGAD sensors. The collected charge and timing resolution of the irradiated LGAD will deteriorate due to the acceptor removal mechanism [12]–[15]. FBK has designed gain layers with different carbon implanted and different depths to enhance the radiation hardness of LGADs [15]–[17]. In this paper, the IHEP-IME designed sensors with the shallow carbon and deeper N++ layer to enhance the radiation hardness. The IHEP-IME sensors were irradiated by the neutron up to $2.5 \times 10^{15} \text{ n}_{\text{eq}}/\text{cm}^2$. IHEP-IME LGAD sensors were designed by the Institute of High Energy Physics (IHEP) and fabricated by the Institute of Microelectronics (IME).

II. PARAMETERS OF THE IHEP-IMEv1 LGAD

The first batch of the IHEP-IME LGADs (IHEP-IMEv1) was fabricated on an 8-inch wafer. The wafer has a $50 \mu\text{m}$ p-type epitaxial layer (active layer) and a $725 \mu\text{m}$ P++ substrate. The IHEP-IMEv1 LGADs have three wafers, wafer1 (W1), wafer7 (W7), and wafer8 (W8). Table I shows the specific parameters of the three wafers. Taking W7 as a reference, W1 has carbon implantation, and W8 has a deeper N+ layer because of higher implantation energy. The resistivity of the active layer of the three wafers is about $1000 \Omega \cdot \text{cm}$. The layout of the single pad IHEP-IMEv1 LGAD is shown in

TABLE I
IMPLANTATION PARAMETERS OF THE W1, W7 AND W8.

Sensors	N++ layer energy (KeV)	P+ layer energy (KeV)	Carbon implantation
W1	40	400	Yes
W7	40	400	No
W8	50	400	No

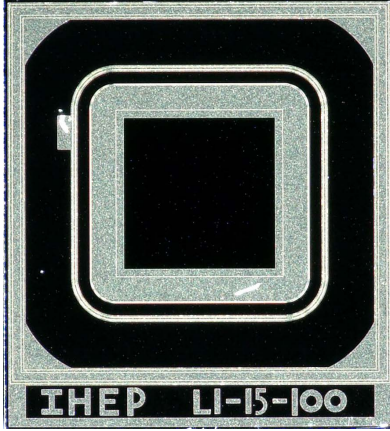


Fig. 2. The layout of IHEP-IMEv1 LGAD sensor.

Fig. 2, the pad size is $1.3 \text{ mm} \times 1.3 \text{ mm}$. The inner metal ring is a pad electrode, and the outer metal ring is a guard ring electrode.

III. NEUTRON IRRADIATION

The IHEP-IMEv1 LGADs were irradiated with neutron at the Jozef Stefan Institute research reactor, which has been used successfully in the past decades to support sensor development [18]. Three irradiation fluences are set, respectively 0.8×10^{15} , 1.5×10^{15} and $2.5 \times 10^{15} \text{ n}_{\text{eq}}/\text{cm}^2$. After irradiation, the $50 \text{ }\mu\text{m}$ LGADs were annealed for 80 min at $60 \text{ }^\circ\text{C}$, which roughly simulates the room temperature annealing at the end of year shut-down period during the operation of the HL-LHC.

IV. EFFECT OF IRRADIATION ON CAPACITANCE AND LEAKAGE CURRENT CHARACTERISTICS

A. Current-Voltage(I-V)

Figure 3 shows the leakage current of IHEP-IMEv1 LGAD sensors in a dark environment at -30°C . Before irradiation, the leakage current of the three sensors at nA level, and breakdown at 86 V (W1), 92 V (W7), and 125 V (W8). The W1 with carbon implantation shows a little lower breakdown voltage. The W8 with a deeper N+ layer has a higher breakdown voltage. When the irradiation fluence up to $2.5 \times 10^{15} \text{ n}_{\text{eq}}/\text{cm}^2$, the W1 has a slightly higher leakage current than W7 and W8, which is about $1 \text{ }\mu\text{A}$ ($59 \text{ }\mu\text{A}/\text{cm}^2$) at 655 V. All the three sensors meets the HGTD requirements ($<125 \text{ }\mu\text{A}/\text{cm}^2$).

B. Capacitance-Voltage(C-V)

LCR meter was used to test the C-V characteristics of the IHEP-IMEv1 LGAD sensors at room temperature. Figure 4

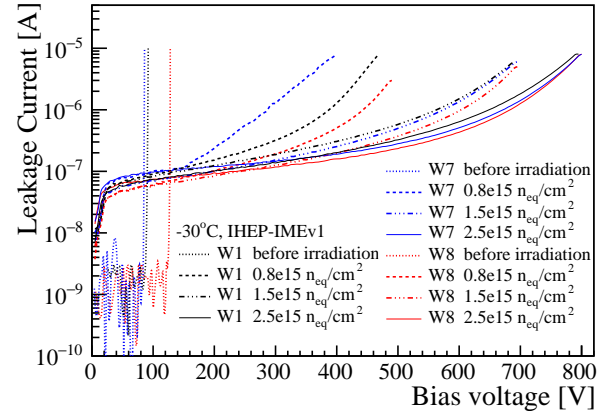


Fig. 3. (color online) I-V curves of IHEP-IMEv1 LGAD sensors at -30°C .

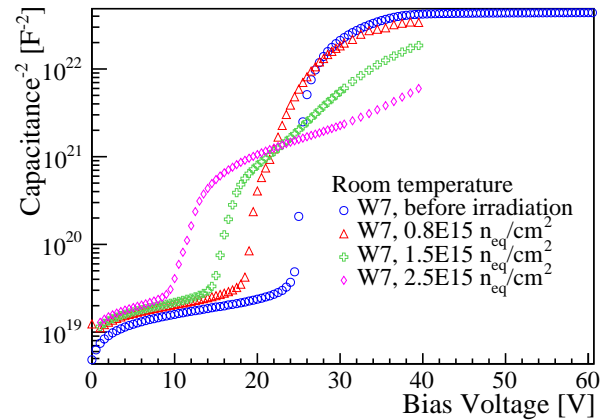


Fig. 4. $1/C^2$ as a function of bias voltage for IHEP-IMEv1 LGAD W7 sensors.

shows the $1/C^2$ as a function of the bias voltage before and after irradiation sensors. As the irradiation fluence increased, the active acceptor of the gain layer is gradually removed, and the gain layer depletion voltage V_{GL} is gradually reduced, as shown in Fig. 5. The gain layer depletion voltage V_{GL} is exponentially dependent on fluence [13]:

$$V_{GL} \approx V_{GL0} \cdot \exp(-c\Phi_{\text{eq}}) \quad (1)$$

where c is the removal constant, V_{GL0} is the initial gain layer depletion voltage. The removal constant values of W1, W7 and W8 were found to be 3.12×10^{-16} , 3.36×10^{-16} and 3.17×10^{-16} respectively. W1 and W8 have smaller removal constants than W7.

V. EFFECT OF IRRADIATION ON THE TIMING RESOLUTION AND COLLECTED CHARGES

A. Beta experiment setup

To study the timing resolution and collected charge, the LGAD sensors were tested with a beta source Sr-90 at -30°C . The LGAD sensor is wire bonded to the readout board and the guard ring is grounded. The readout board is designed by the University of California Santa Cruz (UCSC) [4]. It uses a

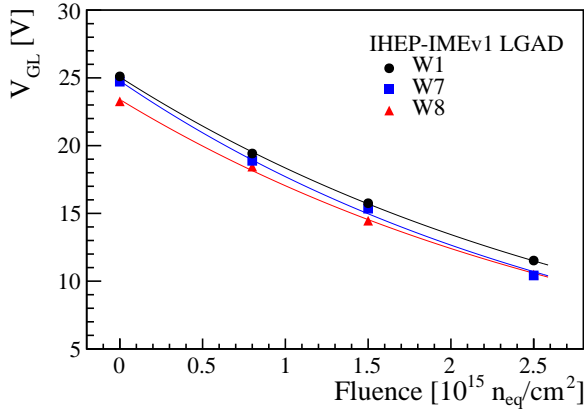


Fig. 5. V_{GL} as a function of irradiation fluence for IHEP-IMEv1 LGAD sensors.

broad band inverting trans-impedance amplifier of 470Ω . This preamplifier is followed by an external second stage amplifier with a gain of 20 dB. Figure 6 shows the beta telescope experiment setup, the lower sensor is used as the trigger for electrons signal in the beta telescope test. The signal pulses from both sensors are recorded by a digital oscilloscope with 40 GS/s sampling rate for offline analysis.

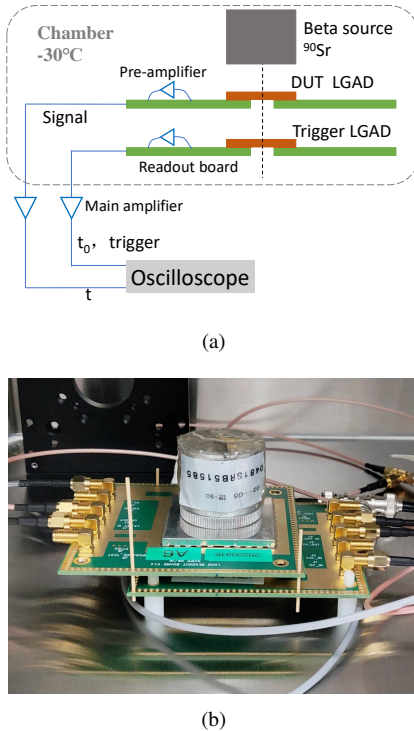


Fig. 6. Beta telescope experiment setup for IHEP-IME sensors. (a) Schematic diagram. (b) Experimental picture.

B. Timing resolution

In the beta test, the timing resolution was obtained from the spread of the flight time Δt of the electron passing through the Device Under Test (DUT) LGAD and the trigger LGAD.

The timing resolution of the DUT sensor could be calculated as the following equation:

$$\sigma_{DUT} = \sqrt{\sigma_{\Delta t}^2 - \sigma_{trigger}^2} \quad (2)$$

In our study, the IHEP-NDLv3 LGAD sensor is used as a trigger LGAD with a timing resolution of 31.2 ps at -30°C [11]. The detailed calculation for timing resolution was described in Ref. [4].

The timing resolution of the IHEP-IMEv1 LGAD sensors before and after irradiation is shown in Fig. 7. Before irradiation, the best timing resolutions of the W8, W7, and W1 are 38 ps, 40 ps, and 48 ps. The timing resolution of the W1 with shallow carbon is worse than the others, which is probably due to the higher leakage current.

After irradiation, the best timing resolutions of the three sensors were obtained at the largest bias voltages which were the critical point before the large increase in dark count. At the irradiation points, $0.8 \times 10^{15} \text{ n}_{eq}/\text{cm}^2$, the timing resolution of W1 is slightly better than those of the other two at most bias voltages. But at the irradiation point, $1.5 \times 10^{15} \text{ n}_{eq}/\text{cm}^2$, the timing resolution of the W7 is the best. At $2.5 \times 10^{15} \text{ n}_{eq}/\text{cm}^2$, the timing resolution of W1 is better than that of W7 at most bias voltage points but is worse than that of W8 and W7 after 760 V. To sum up, it's hard to say which sensor is better only in the point of the timing resolution. However, the performance of the three sensors is significantly different when focusing on the jitter contribution.

The timing resolution mainly consisted of three items, the jitter item, the time walk item, and the landau item as the following equation,

$$\sigma_t^2 = \sigma_{TimeWalk}^2 + \sigma_{Landau}^2 + \sigma_{Jitter}^2 \quad (3)$$

To correct for the time walk due to amplitude variations, the CFD algorithm can be used to calculate the time of electron hitting two LGADs and get the flight time Δt_{Ref} [4]. The jitter could be approximated by the following equation:

$$\sigma_{Jitter} \approx \frac{t_r}{S/N} \quad (4)$$

The t_r is the rise time. The S/N is the signal-to-noise ratio (SNR). As shown in Fig. 8, the rise time didn't change too much with the increase of the irradiation fluences after $0.8 \times 10^{15} \text{ n}_{eq}/\text{cm}^2$. Before irradiation, the rise time of different sensors are different when the sensors were biased to the same voltage. After irradiation, the rise time of the three sensors became almost the same even with different bias voltage which is about 0.46 ns. The almost unchanged rise time is assumed to be due to the saturation of the electron drift velocity induced by the high bias voltage applied ($> 200 \text{ V}$) after irradiation.

According to the equation 4, the jitter could be calculated and the results are shown in Fig. 9. After irradiation, the deterioration of the jitter of the W1 with shallow carbon is less than those of the W7 and W8. The deterioration of the jitter of W8 with a deeper N++ layer is the largest.

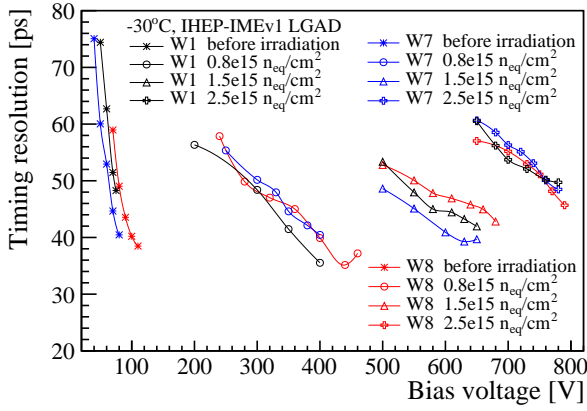


Fig. 7. (color online) Time resolution as a function of bias voltage for IHEP-IMEv1 LGADs before and after irradiation at -30°C

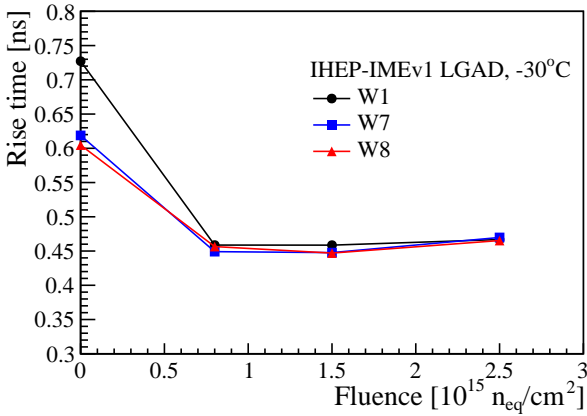


Fig. 8. The rise time of the three sensors with different irradiation fluences.

C. Collected charge

The collected charge for each signal pulse is calculated by dividing the integration of the pulse by the gain of amplifiers. The distribution of the charge collection is fitted with the Landau-Gauss convolution to get the charge most probability value (MPV) for a certain bias.

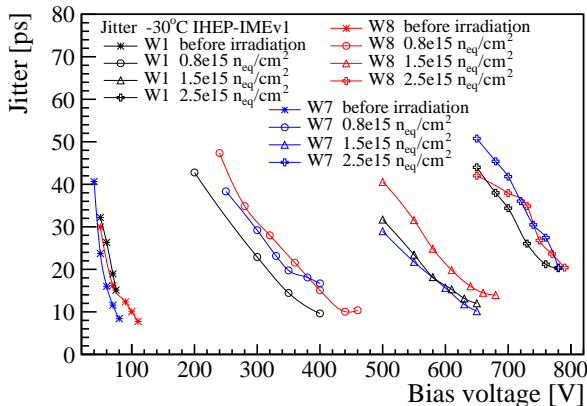


Fig. 9. Jitter before and after irradiation

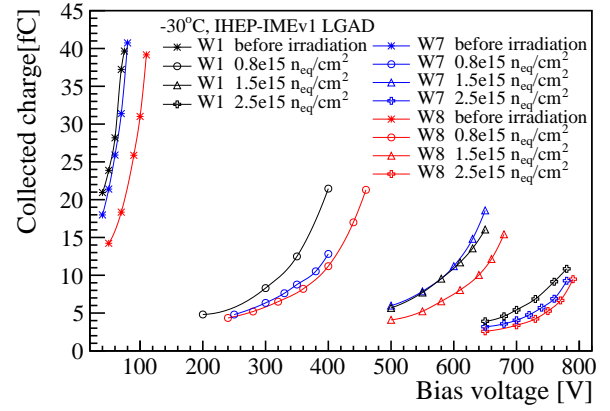


Fig. 10. (color online) The collected charge as a function of bias voltage for IHEP-IMEv1 LGADs before and after irradiation at -30°C

TABLE II
THE OPERATING RANGE OF THE W1, W7 AND W8 AFTER
 $2.5 \times 10^{15} \text{ n}_{\text{eq}}/\text{cm}^2$ NEUTRON IRRADIATION.

Sensors	Operating voltage range [V]	Operating range width [V]
W1	655-705	50
W7	700-725	25
W8	725-730	5

The collected charge of the IHEP-IMEv1 sensors measured by the beta telescope before and after irradiation is shown in Fig. 10. Before irradiation, all three sensors have a very high collected charge, which is about 40 fC. After irradiation, the collected charge of the three sensors could meet the HGTD requirements ($>4 \text{ fC}$ after $2.5 \times 10^{15} \text{ n}_{\text{eq}}/\text{cm}^2$ irradiation fluence). The largest collected charges of all three sensors decreased. However, the deterioration of the collected charge of W1 is the smallest, while the deterioration of W8 is the largest. It indicates that the application of the shallow carbon could help increase the collected charge at the same irradiation fluence. While increase the injection energy of the N^{++} layer could decrease the collected charge after irradiation.

VI. OPERATING BIAS VOLTAGE RANGE AFTER $2.5 \times 10^{15} \text{ n}_{\text{eq}}/\text{cm}^2$ IRRADIATION

After $2.5 \times 10^{15} \text{ n}_{\text{eq}}/\text{cm}^2$ irradiation, the sensors should operate on the bias voltage range which satisfied the HGTD project requirements (The timing resolution $< 70 \text{ ps}$; The collected charge $> 4 \text{ fC}$; The leakage current $< 125 \mu\text{A}/\text{cm}^2$ ($2.1 \mu\text{A}$)).

Table II shows the operating bias voltage range of the three sensors. The operating range of W1 with shallow carbon is 2 times wider than that of the W7 and 10 times wider than that of W8. Also, W1 could work at the lowest bias voltage compared with the other two sensors, which could help reduce the single event burnout observed in the testbeam. At the point of the operating range, the shallow carbon could increase the radiation hardness while the deeper N^{++} will weaken the radiation hardness.

VII. CONCLUSION

The IHEP-IMEv1 LGAD sensors were designed by IHEP and fabricated by IME with 50 μm epitaxial layer. We studied the radiation hardness of the three sensors with or without the shallow carbon and the deep N++ layer. The three sensors were irradiated with different neutron fluence, $0.8 \times 10^{15} \text{ n}_{\text{eq}}/\text{cm}^2$, $1.5 \times 10^{15} \text{ n}_{\text{eq}}/\text{cm}^2$ and $2.5 \times 10^{15} \text{ n}_{\text{eq}}/\text{cm}^2$. The leakage current, timing resolution and collected charge are measured before and after irradiation.

The W1 with shallow carbon showed the most promising radiation hardness. After $2.5 \times 10^{15} \text{ n}_{\text{eq}}/\text{cm}^2$ irradiation, the collected charge is the largest at the same bias voltage and achieve 4 fC at the lowest bias voltage (655V). The operating voltage range is 655-705 V which is the widest and the lowest compared with the ranges of the other two designs. The timing resolution of W1 from the beta test is slightly lower than the other two designs at some bias voltages while the jitter contribution of W1 is the smallest at the same bias voltage. The acceptor removal rate is 3.12×10^{-16} and the smallest. But the leakage current of W1 is the largest before and after irradiation due to the shallow carbon. The W8 with a deeper N++ layer showed the worst radiation hardness. After $2.5 \times 10^{15} \text{ n}_{\text{eq}}/\text{cm}^2$ irradiation, the collected charge is the smallest at the same bias voltage and achieve 4 fC at the highest bias voltage, 725V. The operating bias voltage range is 725-730 V which is the narrowest and highest. The jitter contribution of W8 is the largest.

In summary, the leakage current, collected charge, and timing resolution of the three sensors of IHEP-IMEV1 all meet the HGTD requirements ($125 \mu\text{A}/\text{cm}^2$, $>4 \text{ fC}$ and $<70 \text{ ps}$ after $2.5 \times 10^{15} \text{ n}_{\text{eq}}/\text{cm}^2$ irradiation fluence). Before irradiation, the W1 sensor with shallow carbon showed the worst timing performance and moderate collected charge. However, after irradiation, the W1 sensor showed the best irradiation hardness and W8 with a deeper N++ layer showed the worst irradiation hardness. In our next prototype, we are going to vary the carbon dose and the depth to improve the irradiation hardness further.

ACKNOWLEDGEMENT

This work was supported by the National Natural Science Foundation of China (No.11961141014), the State Key Laboratory of Particle Detection and Electronics (No.SKL PDE-ZZ-202001), the Hundred Talent Program of the Chinese Academy of Sciences (Y6291150K2), the CAS Center for Excellence in Particle Physics (CCEPP), the Scientific Instrument Developing Project of the Chinese Academy of Sciences (No.ZDKYYQ20200007).

REFERENCES

- [1] ATLAS Collaboration, Technical Design Report: A High-Granularity Timing Detector for the ATLAS Phase-II Upgrade (CERN-LHCC-2020-007 ; ATLAS-TDR-031). <https://cds.cern.ch/record/2719855?ln=en>
- [2] H. F-W Sadrozinski, et al., 4D tracking with ultra-fast silicon detectors, Rep. Prog. Phys. 81 026101 <https://doi.org/10.1088/1361-6633/aa94d3>
- [3] CERN, High-Luminosity Large Hadron Collider (HL-LHC): Preliminary Design Report (CERN-2015-005). <http://cds.cern.ch/record/2116337>

- [4] N. Cartiglia, et al., Beam test results of a 16 ps timing system based on ultra-fast silicon detectors, Nucl. Instrum. Methods Phys. Res. A, 850 (2017) 83-88. <https://doi.org/10.1016/j.nima.2017.01.021>
- [5] G. Kramberger, et al., Radiation hardness of thin Low Gain Avalanche Detectors, Nucl. Instrum. Methods Phys. Res. A, 891 (2018) 68-77. <https://doi.org/10.1016/j.nima.2018.02.018>
- [6] Y. Zhao, et al., Comparison of 35 and 50 μm thin HPK UFSD after neutron irradiation up to $6 \times 10^{15} \text{ n}_{\text{eq}}/\text{cm}^2$, Nucl. Instrum. Methods Phys. Res. A, 924 (2019) 387-393. <https://doi.org/10.1016/j.nima.2018.08.040>
- [7] J. Lange, et al., Gain and time resolution of 45 μm thin low gain avalanche detectors before and after irradiation up to a fluence of $10^{15} \text{ n}_{\text{eq}}/\text{cm}^2$, J. Instrum. 12 (5) (2017) P05003. <https://doi.org/10.1088/1748-0221/12/05/P05003>
- [8] X. Shi, et al., Radiation campaign of HPK prototype LGAD sensors for the High-Granularity Timing Detector (HGTD), Nucl. Instrum. Methods Phys. Res. A, 979 (2020) 164382. <https://doi.org/10.1016/j.nima.2020.164382>
- [9] M. Wiehe, et al., Study of the radiation-induced damage mechanism in proton irradiated low gain avalanche detectors and its thermal annealing dependence, Nucl. Instrum. Methods Phys. Res. A, 986 (2021) 164814. <https://doi.org/10.1016/j.nima.2020.164814>
- [10] Y. Y. Fan, et al., Radiation hardness of the low gain avalanche diodes developed by NDL and IHEP in China, Nucl. Instrum. Methods Phys. Res. A, 984 (2020) 164608. <https://doi.org/10.1016/j.nima.2020.164608>
- [11] M. Li, et al., The performance of IHEP-NDL LGAD sensors after neutron irradiation, J. Instrum. 16(08) (2021) P08053. <http://doi.org/10.1088/1748-0221/16/08/P08053>
- [12] M. Moll, Displacement Damage in Silicon Detectors for High Energy Physics, IEEE Transactions on Nuclear Science, 65 (2018) 1561-1582. <https://doi.org/10.1016/j.nima.2018.11.121>
- [13] G. Kramberger, et al., Radiation effects in Low Gain Avalanche Detectors after hadron irradiations, J. Instrum. 10(07)(2015) P07006 <https://doi.org/10.1088/1748-0221/10/07/P07006>
- [14] S. O. Ugobono, et al., "Radiation Tolerance of Proton-Irradiated LGADs, IEEE Transactions on Nuclear Science, 65 (2018) 1667-1675. <https://doi.org/10.1109/TNS.2018.2826725>
- [15] M. Ferrero, et al., Radiation resistant LGAD design, Nucl. Instrum. Methods Phys. Res. A, 919 (2019) 16-26. <https://doi.org/10.1016/j.nima.2018.11.121>
- [16] S. M. Mazza, Overview of radiation resistant LGAD designs, CPAD workshop, Virtual, 2021. https://indico.fnal.gov/event/46746/contributions/210257/attachments/141110/177757/090321_CPAD_LGAD_radhard.pdf
- [17] G. Paternoster, New developments in Ultra Fast Silicon Detectors at FBK, 31th RD50 Workshop, CERN, Geneva, 2017. https://indico.cern.ch/event/663851/contributions/2787294/attachments/1562040/2484362/RD50_17_11_ext.pdf
- [18] L. Snoj, et al., Computational analysis of irradiation facilities at the JSI TRIGA reactor, Nucl. Instrum. Methods Phys. Res. A, 70 (2012) 483-488. <https://doi.org/10.1016/j.nima.2011.11.042>